# Multiparametric MRI Prostate Cancer Analysis via a Hybrid Morphological-Textural Model

Andrew Cameron, Amen Modhafar, Farzad Khalvati, Dorothy Lui,
Mohammad J. Shafiee, Alexander Wong, Masoom Haider

*Abstract*— **Multiparametric MRI has shown considerable promise as a diagnostic tool for prostate cancer grading. Diffusion-weighted MRI (DWI) has shown particularly strong potential for improving the delineation between cancerous and healthy tissue in the prostate gland. Current automated diagnostic methods using multiparametric MRI, however, tend to either use low-level features, which are difficult to interpret by radiologists and clinicians, or use highly subjective heuristic methods. We propose a novel strategy comprising a tumor candidate identification scheme and a hybrid textural-morphological feature model for delineating between cancerous and non-cancerous tumor candidates in the prostate gland via multiparametric MRI. Experimental results using clinical multiparametric MRI datasets show that the proposed strategy has strong potential as a diagnostic tool to aid radiologists and clinicians identify and detect prostate cancer more efficiently and effectively.**

## I. Introduction

Prostate cancer is the most-diagnosed form of cancer in Canadian men, with an estimated 23,600 new cases projected to be diagnosed in 2013 with 3,900 of those cases expected to result in death [1]. Although it is the third leading cause of cancer death in men, prostate cancer has good prognosis if detected early [2]. Effective and reliable screening methods for prostate cancer are therefore very important.

Several different methods are currently used to detect prostate cancer, though none are widely-accepted or standardized. The prostate-specific antigen (PSA) test measures the concentration of specific markers in the patient's blood where in high levels indicate high risk for prostate cancer. However, use of the PSA test has been criticized for having an unacceptably high occurrence of false positives, causing healthy patients to undergo expensive and uncomfortable confirmatory tests [3], [4]. Following a positive PSA test, a systematic transrectal ultrasound (TRUS) guided biopsy is undertaken where multiple samples are collected. Although core biopsies are very accurate, they are intrinsically invasive, causing significant discomfort to the patient and exposing him to possibly unnecessary surgical risk. Furthermore, TRUS cannot detect isoechoic tumors making TRUS-guided biopsies even more difficult.

Multiparametric magnetic resonance imaging (MRI) has shown considerable promise for diagnosis, especially the combination of T2-weighted MRI (T2w) and diffusion-weighted MRI (DWI). T2w affords doctors the ability to see relatively high-resolution imagery of the prostate and surrounding tissue, while allowing detection of subtle structural features. Recent research has focused on DWI and the DWI-derived Apparent Diffusion Coefficient (ADC), which quantifies the diffusion of water molecules through tissue and has been shown to delineate between healthy and cancerous tissue [5]. Example multiparametric MRI scans are shown in Figure 1. It can be observed that each modality provides different information about the prostate gland, which is useful in aiding radiologists and clinicians in the clinical decision support process.

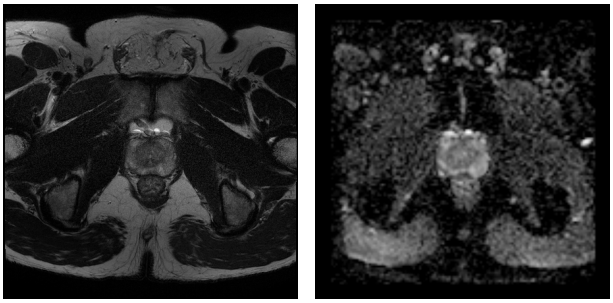

(a) T2w (b) DWI: apparent diffusion coefficient (ADC)

Fig. 1: Example multiparametric MRI slices of the same prostate gland, using T2w and diffusion-weighted imaging (DWI). Each modality provides different information about the prostate gland to aid in the clinical decision support process.

Detecting prostate cancer automatically has been a popular area of research and to date, these methods have focused exclusively on low-level features. Conventional multiparametric MRI prostate cancer analysis approaches use one or more of the MRI modality values or derived values, including ADC and T2w, with no complementary high-level features [6]. Published values for classification accuracy using these low-level features ranges from 64% to 89% [5]–[10].

More sophisticated approaches calculate multiple low-level features and then combine them using an ensemble classification strategy. Low-level features considered in such approaches include statistical features (e.g. local variance) and change-of-basis features such as Gabor filter coefficients [11], discrete cosine transform (DCT) coefficients and textural features (both first and second-order), such as those

A. Cameron, D. Lui, M. Shafiee, and A. Wong are from the Department of Systems Design Engineering at the University of Waterloo, Waterloo, Ontario, Canada; A. Modhafar, F. Khalvati, and M. Haider are from the Department of Medical Imaging at Sunnybrook Health Sciences Centre, Toronto, Ontario, Canada.

978-1-4244-7929-0/14/$26.00 ©2014 IEEE

derived from co-occurrence matrices (CMs). Chan et al. [7] reported that compared to using MRI intensity features exclusively, DCT and CM features improved accuracy between 6.2% and 11.0% (accuracy of 72.9% without those features, and 79.1% – 83.9% with them). Madabhushi et al. [11] reported a Positive Predictive Value (PPV) of approximately 21% when using a combination of first and second-order statistical features, gradient features, and Gabor features within an ensemble classification framework. However, since the low-level features lack semantic meaning, the classification decisions made by such approaches are difficult to justify to radiologists and clinicians, who typically use subjective heuristics to diagnose patient cases. Although the latter approach is easy to understand and justify, its subjective nature makes it highly inconsistent.

High-level features on the other hand have been used in detecting and localizing prostate cancer; however, their use is still limited. Naik et al. [12] demonstrated that classifiers built using high-level features designed using domain knowledge are effective at diagnosing prostate tissue as cancerous and distinguishing cancerous tissue between two grades on the Gleason scale, with classification accuracy in the range of 86–95%. Unfortunately, this method uses high-resolution imagery from scanned histology slides, necessitating invasive surgery. Haider et al. [6] described a scoring scheme for diagnosing prostate cancer based on high-level features observed in T2w and ADC imagery. However, these features are not easily quantifiable and are intended for use by trained radiologists and not classification algorithms.

By examining how existing low and high-level feature models are used, we motivate the need for a quantitative high-level feature model. In this paper, we investigate the use of high-level features, such as tumor morphology, for detection of prostate cancer. With intuitive features, classification decisions can be more easily justified and explained to medical practitioners, while simultaneously providing more consistently quantifiable measures. In this work, we introduce a novel strategy for computer-aided prostate cancer analysis that combines i) a tumor candidate identification scheme based on multiparametric MRI and morphology, and ii) a hybrid textural-morphological feature model for delineating between cancerous and non-cancerous tumors amongst the tumor candidates.

## II. Hybrid Textural-Morphological Model

In the proposed method, initial identification of candidate tumor regions is automatically performed using multiparametric MRI and morphology. After candidate regions are identified by the automatic tumor candidate identification algorithm, textural and morphological features are extracted to form a hybrid morphological-textural feature model that combines high-level morphological features with low-level textural features.

### A. Automatic tumor candidate identification

Tumor candidate regions were identified automatically in the proposed system using guidelines for clinical multiparametric MRI prostate cancer screening by a radiologist [6]. Tissues satisfying these criteria were grouped into connected regions and analyzed further with the textural-morphological feature model detailed below. In particular, diffusion characteristics and morphology were used to automatically identify candidate regions in the proposed system.

As low ADC values are associated with tumorous tissue [6], tissue with ADC values below a particular threshold were automatically identified by the proposed system as possible tumor candidates. Considering that the priority of the candidate identification phase is to highlight regions for consideration, rather than to eliminate them, the threshold value used in [6] was relaxed to capture more regions. All voxels with an ADC value less than $1000 \times 10^{-6}$ $\mathrm{mm}^2/\mathrm{s}$ were flagged as possible tumor candidates. These flagged voxels are then grouped into connected regions, and a second phase is used in the automatic tumor candidate identification algorithm to take morphology into account. In particular, size is taken into consideration and all connected regions larger than $1\,\mathrm{mm}^2$ were considered as the final set of tumor candidate regions.

### B. Textural features

After the tumor candidate regions have been identified, a set of low-level texture features were computed for those regions as part of the proposed hybrid morphological-texture feature model. Texture features were included to capture the different textural characteristics between cancerous and healthy tissue [11]. T2w intensity values were included as an initial feature. In addition, a series of local statistical features and Gabor filter responses were extracted from the T2w intensity images in order to quantify textural characteristics of imaged tissue [11]. Texture features were also computed using ADC values and likewise augmented with the ADC map as a further feature. Feature values for each region were obtained by averaging textural filter responses over the region.

The statistical features consisted of the median, standard deviation, and average deviation first-order features as well as the contrast, correlation, and homogeneity second-order features. All were computed using $3 \times 3$ and $5 \times 5$ voxel regions around the voxel of interest [11].

Gabor filters were applied at a combination of scales and orientations totalling 18 features, corresponding to the scales $u_0 = \{16\sqrt{2}, 32\sqrt{2}, 64\sqrt{2}\}$ and the orientations $\theta = n\pi/6, n = 0 \ldots 6$.

### C. Morphological features

In the proposed hybrid morphological-textural feature model, a set of high-level features are also computed to characterize the morphology of the tumor candidate region. Morphological features capture structural information about a candidate region by applying operations which smooth the shape of the region boundary. Regions with little morphological irregularity undergo little change with the smoothing operator, while regions with highly irregular shapes will see a drastic difference.


(a) Morphological area feature

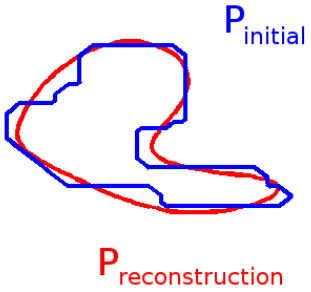


(b) Morphological perimeter feature

Fig. 2: Illustrations of the morphological features. In 2a, the area feature illustration, purple and orange contours denote the morphological opening and closing, respectively, of a candidate region. The large difference in areas between the contours results in a high feature value for this region.
In 2b, the perimeter feature illustration, a candidate region contour, shown in blue, has a perimeter similar in length to that of the region's low-frequency Fourier reconstruction, shown in red, resulting in a low feature value for this region.

The first feature in this group is the normalized difference in area between the morphological closing of the region and the morphological opening of the region, using an identical disk structuring element for both operations [13]:

$$f_1^B = \frac{A_{closed} - A_{opened}}{A_{initial}} \quad (1)$$

Here, $A$ denotes the area of a region. Peaks and valleys in the border of the region will cause the area to increase after closing, while it will decrease after opening (i.e., $A_{closed} \geq A_{opened}$); therefore, regions with very irregular borders will have a greater difference between these two values, and the feature value will be greater. Smaller feature values then correspond to regions with borders which do not feature sharp peaks and valleys. An example region is shown in Fig. 2a.

The second morphological feature compares the length of the region's perimeter before and after eliminating high-frequency components in the Fourier space, and normalizing the difference:

$$f_2^B = \frac{|P_{initial} - P_{reconstruction}|}{P_{initial}}, \quad (2)$$

where each $P$ is the perimeter of the region denoted by its subscript. Since high-frequency components capture rapid changes in the shape of the region, this feature will be greater for regions with rapidly-varying boundaries than for those with smooth, slowly-varying boundaries [13]. An example region is shown in Fig. 2b.

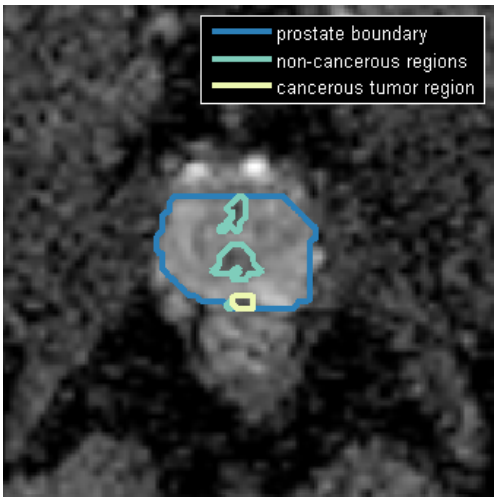


Fig. 3: An example patient case with contours for the prostate gland (blue), non-cancerous regions (green), and cancerous tumor region (yellow) overlaid on the apparent diffusion coefficient (ADC) map of the prostate gland. Note that the yellow and green regions exhibit similar ADC values, indicating that ADC alone is insufficient for delineation between cancerous tumors and non-cancerous regions.

## III. Experimental Results

Clinical multiparametric MRI was acquired from five patients (ages 54-81, median 63). Informed consent was obtained from all patients, and approval for this study was obtained from the ethics review board of Sunnybrook Health Sciences Centre. All acquisitions were made at Sunnybrook Health Sciences Centre, in Toronto, using a Philips Achieva 3.0 T machine with a Display Field Of View (DFOV) of $20 \times 20$ cm$^2$, resolution of $1.5625 \times 1.5625 \times 3$ mm$^3$. Echo Times (TE) were 61 ms and Repetition Times (TR) were between 6173 ms and 6693 ms, with a median of 6173 ms. A radiologist with 18 and 13 years of experience interpreting body and prostate MRI, respectively, manually confirmed twenty-five regions as cancerous. Figure 3 shows an example patient case with contours drawn around cancerous and non-cancerous regions for the sake of illustration. Both cancerous and non-cancerous regions in this image exhibit similar ADC values, making classification using ADC value alone prone to error.

Region labels were used as ground truth to train Naive Bayes classifiers in a leave-one-out cross-validation scheme. Each region was held out while the remaining regions were used to train a classifier, which was then used to predict the held-out region's label. Classification performance was assessed by evaluating the accuracy, sensitivity, and specificity of these predictions.

### A. Feature model performance

The performance of each feature set on the training and classification process described above are shown in Figure 4.

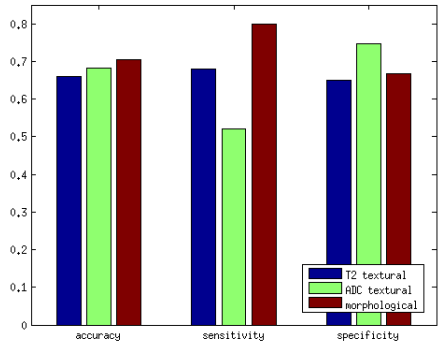


Fig. 4: Classification performance (accuracy, sensitivity, and specificity) of textural and morphological features separately.

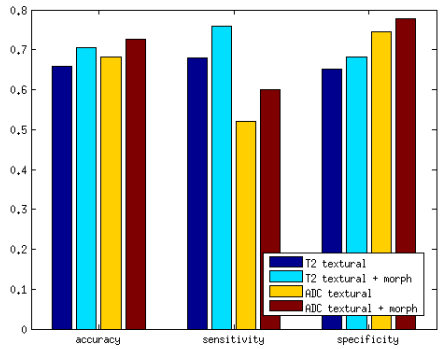


Fig. 5: Classification performance (accuracy, sensitivity, and specificity) of textural features augmented with morphological features

In addition to the T2w-based textural features, a set of similar texture features was computed using ADC intensity values. Although the ADC-based textural features achieve slightly higher accuracy compared to the T2w textural features, they suffer from a drastic loss in sensitivity.

The benefit of adding high-level morphological features to construct hybrid textural-morphological feature models is clear from Figure 5. Performance of textural features is improved with the addition of the morphological features, whether textural features are computed on T2w or ADC images. Therefore, in addition to being easier to interpret by radiologists, the integration of high-level morphological features also improved classification performance.

## IV. Conclusions

A novel hybrid feature model was proposed, which departs from current methods by combining the use of multiparametric MRI with low-level textural and high-level morphological properties. This hybrid morphological-textural feature model appears to offer improved diagnostic power compared to using texture features alone, as well as being easier to interpret by radiologists.

### A. Recommendations and Future Work

As these results are preliminary, further validation with larger datasets is warranted. At this point, false positives and false negatives should be carefully examined in the feature space to determine if additional intuitive features might reduce misclassifications. As well, user acceptance testing in a clinical environment is needed to ensure the intuitive features correspond with the perception of expert diagnosticians, and could be used to inform the design of new intuitive features.

## Acknowledgment

The authors would like to thank the Canada Research Chairs program, The Natural Sciences and Engineering Research Council of Canada, and the Ontario Ministry of Research and Innovation for supporting this work.

## References

[1] Canadian Cancer Society, "Prostate cancer statistics." [Online]. Available: http://www.cancer.ca/en/cancer-information/cancer-type/prostate/statistics/?region=sk

[2] Prostate Cancer Canada Network, "Early detection guidelines," 2012.

[3] P. R. Carroll, "Early detection of prostate cancer," *Commun Oncol*, vol. 7, pp. 25 – 27, 2010.

[4] I. M. Thompson, D. K. Pauler, P. J. Goodman, C. M. Tangen, M. S. Lucia, H. L. Parnes, L. M. Minasian, L. G. Ford, S. M. Lippman, E. D. Crawford, J. J. Crowley, and C. A. C. Jr., "Prevalence of prostate cancer among men with a prostate-specific antigen level $\leq$ 4.0 ng per mililiter," *N Engl J Med*, vol. 350, pp. 2239 – 2246, 2004.

[5] S. Ozer, M. A. Haider, and D. Langer, "Prostate cancer localization with multispectral MRI based on relevance vector machines," in *2009 IEEE International Symposium on Biomedical Imaging: From Nano to Macro*, 2009, pp. 73–76.

[6] M. A. Haider, T. H. van der Kwast, J. Tanguay, A. J. Evans, A.-T. Hashmi, G. Lockwood, and J. Trachtenberg, "Combined T2-weighted and diffusion-weighted MRI for localization of prostate cancer." *AJR. American journal of roentgenology*, vol. 189, no. 2, pp. 323–8, Aug. 2007.

[7] I. Chan, W. Wells, R. V. Mulkern, S. Haker, J. Zhang, K. H. Zou, S. E. Maier, and C. M. C. Tempany, "Detection of prostate cancer by integration of line-scan diffusion, T2-mapping and T2-weighted magnetic resonance imaging; a multichannel statistical classifier," *Medical Physics*, vol. 30, no. 9, p. 2390, 2003.

[8] X. Liu, D. Langer, M. A. Haider, and Y. Yang, "Prostate cancer segmentation with simultaneous estimation of Markov random field parameters and class," *Medical Imaging,*, vol. 28, no. 6, pp. 906–915, 2009.

[9] D. L. Langer, T. H. van der Kwast, A. J. Evans, J. Trachtenberg, B. C. Wilson, and M. A. Haider, "Prostate cancer detection with multi-parametric MRI: logistic regression analysis of quantitative T2, diffusion-weighted imaging, and dynamic contrast-enhanced MRI." *Journal of magnetic resonance imaging : JMRI*, vol. 30, no. 2, pp. 327–34, Aug. 2009.

[10] S. Ozer, D. L. Langer, X. Liu, M. a. Haider, T. H. van der Kwast, A. J. Evans, Y. Yang, M. N. Wernick, and I. S. Yetik, "Supervised and unsupervised methods for prostate cancer segmentation with multispectral MRI," *Medical Physics*, vol. 37, no. 4, pp. 1873–1883, 2010.

[11] A. Madabhushi, M. D. Feldman, D. N. Metaxas, J. Tomaszeweski, and D. Chute, "Automated detection of prostatic adenocarcinoma from high-resolution ex vivo MRI." *IEEE transactions on medical imaging*, vol. 24, no. 12, pp. 1611–25, Dec. 2005.

[12] S. Naik, S. Doyle, M. Feldman, and J. Tomaszewski, "Gland segmentation and computerized gleason grading of prostate histology by integrating low-, high-level and domain specific information," *MIAAB*, pp. 1–8, 2007.

[13] R. Amelard, A. Wong, and D. A. Clausi, "Extracting Morphological High-Level Intuitive Features (HLIF) for Enhancing Skin Lesion Classification," in *34th Annual International Conference of the IEEE Engineering in Medicine and Biology Society*, San Diego, 2012, pp. 4458 – 4461.